CHAPTER 6

GROUND PENETRATING RADAR (GPR) STUDIES ALONG VIGODI-GUGRIANA-KHIRASRA-NETRA FAULT SYSTEM (VGKNFS)

2D GPR surveys were carried out with a view to map the continuity of the VF and WVF buried below patchy alluvial cover, to reveal their shallow subsurface nature and to further strengthen our field observations indicating the changing slip-sense. It is to be noted that all the four sectors were not worked for GPR surveys.

Radargrams were obtained in continuous mode by using shielded monostatic 200 MHz frequency antenna. It provided satisfactory results in terms of both the depth of penetration (6–8 m) and resolution required to study the near surface nature of faults. The position of the fault was confirmed by observing the changes in reflector pattern Dielectric constant was kept 7 with time window (range) of 125-150 ns during survey operation. The VF protrudes from the surrounding cultivated soil surface as a small ~0.5 m high striated fault plane in Bhuj sandstone. 17 m long profile was acquired in N240° direction perpendicular to the NW striking fault. The NNW striking, ~3 m high WVF is exposed in Bhuj sandstone, cross-cutting the NE flowing Makdawali river. GPR survey was conducted in the riverbed of the Makdawali river, with 15 m long profile in N260° direction.

The GPR studies along VGKNFS are described below. The GPR sites 1–9 are located along the KMF, which are described in the previous chapter.

WEST VIGODI FAULT (WVF) AND ASSOCIATED SUBSIDIARY FAULTS

Site 10

The processed radargram shows SW dipping WVF at ~11 m horizontal distance (Figs. 6.1a-d). The clear lateral discontinuity of reflectors passing across the fault plane can be observed. The near surface fault geometry and slip-sense inferred from the radargram correlates well with the nearby surficial fault exposure. From NE to SW, thinning of reflectors is observed across the fault plane. The radargram can be divided into five distinct radar reflection packages demarcated based on the reflector pattern response:

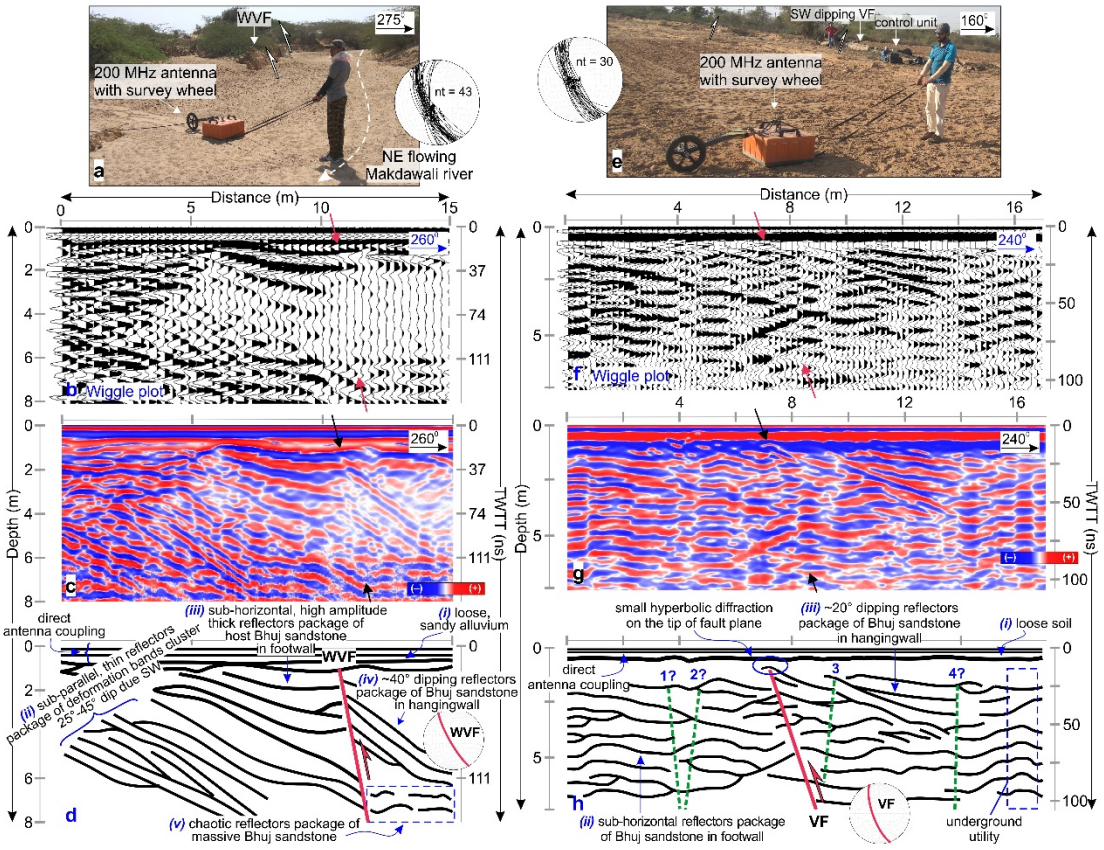

Fig. 6.1. (a)-(d) 15 m long, SW oriented GPR profile acquired across the NNW striking WVF. Transect is taken in the riverbed of NE flowing Makdawali river. (e)-(h) 17 m long, SW oriented GPR profile recorded across the NW striking VF. See geological map of the study area in Fig. 3.1 for location of GPR survey sites. Axis on left side shows penetration depth in meters and on right side two way travel time (TWTT) in ns is denoted. The upper axis shows profile length in meters. Inset stereonet in Figs. (d) and (h) show the geometry of WVF and VF inferred from the radargram.

(i) Long, continuous, horizontal reflectors

At 0-37 ns depth interval, the top segment is occupied by long, continuous, thick reflectors belonging to loose, sandy alluvium in the riverbed (Fig. 6.1d).

(ii) Moderate to gently, SW dipping reflectors package in footwall

GPR survey also picked the hard, compacted, cluster of deformation bands (dies out along the fault) as their subtle dielectric contrast with the host, friable Bhuj sandstone (Fig. 6.1d). The deformation bands cluster is marked by closely-spaced, sub-parallel, thin, 25-45° dipping reflectors, which continue up to 7 m horizontal distance. It has to be noted that each, wavy, undulating reflector pattern within the package may/may not mark the individual strand of deformation bands cluster.

(iii) Sub-horizontal reflectors package in footwall

In the interval of 5-10 m horizontal distance, the amplitude of reflectors suddenly increases. This radar reflection package encompasses the sub-horizontal, high amplitude, thick reflectors of massive, host Bhuj sandstone (devoid of any deformation bands) in the footwall that are truncated along the SW dipping fault (Fig. 6.1d).

(iv) SW dipping reflectors package in hangingwall

In the hangingwall, in the interval of 11-15 m horizontal distance, ~40° dipping towards SW, thin reflectors of Bhuj sandstone ride over (displaced upward) the SW dipping/sub-horizontal thick reflectors in the footwall (radar reflectors package (iii)) indicating reverse dip-slip along the fault (Fig. 6.1d). Along with the sheer change in dip of reflectors across the fault, there is a sudden decrease in the amplitude of radar reflections from reflectors package (iii) to (iv), due to deformation in the damage zone. The low amplitude radar signals can be clearly observed in the wiggle traces (Fig. 6.1b).

(v) Chaotic radar reflection package

Towards the SW side, in the deeper segment of radargram, a package of thin, small, discontinuous yet (sub-)horizontal reflectors with no specific shape can be observed in the hangingwall block of the WVF between 6-8 m depth (110-150 ns depth range) (highlighted in the dashed box area in Fig. 6.1d).

Site 11

~3 km east of Rawapar, the SW dipping WVF is exposed in Bhuj sandstone in the NE flowing Makdawali river (Fig. 6.2). ~7.15 km long, WVF bifurcates from the VF at ~2.25 km NNW of sites 11. The Makdawali river has been deflected, where the WVF crosses the river. The two E and NE flowing tributaries meet where the fault passes through, the river then flows in NE direction. Fault-slip analysis results suggest that the WVF has generated under pure compressive stress regime with SHmax trending in N48° E direction.

The 2D GPR survey is carried out at site 11 with a view to map the shallow subsurface occurrence of NW trending WVF, N-NE trending cluster of deformation bands and to further confirm our paleostress analysis results suggesting reverse dip-slip movement (Fig. 6.2).

The 200 MHz frequency antenna with attached survey wheel is used to collect the radargrams in continuous mode. The antenna is dragged over the riverbed composed of loose, sandy alluvium. While carrying out the survey operation, at 60 m horizontal

distance, the computer attached to the SIR-20 unit crashed and therefore, further mapping the deformation bands cluster could not be continued. The dielectric constant is kept 7 with depth range of 100 ns and the depth of penetration achieved is 6 m. The marker is assigned manually to the radargram when the antenna crossed the approximate position of the WVF as well as of the cluster of deformation bands. The length of the profile is 60 m and the survey-line is in N275° direction perpendicular to the NW trending WVF.

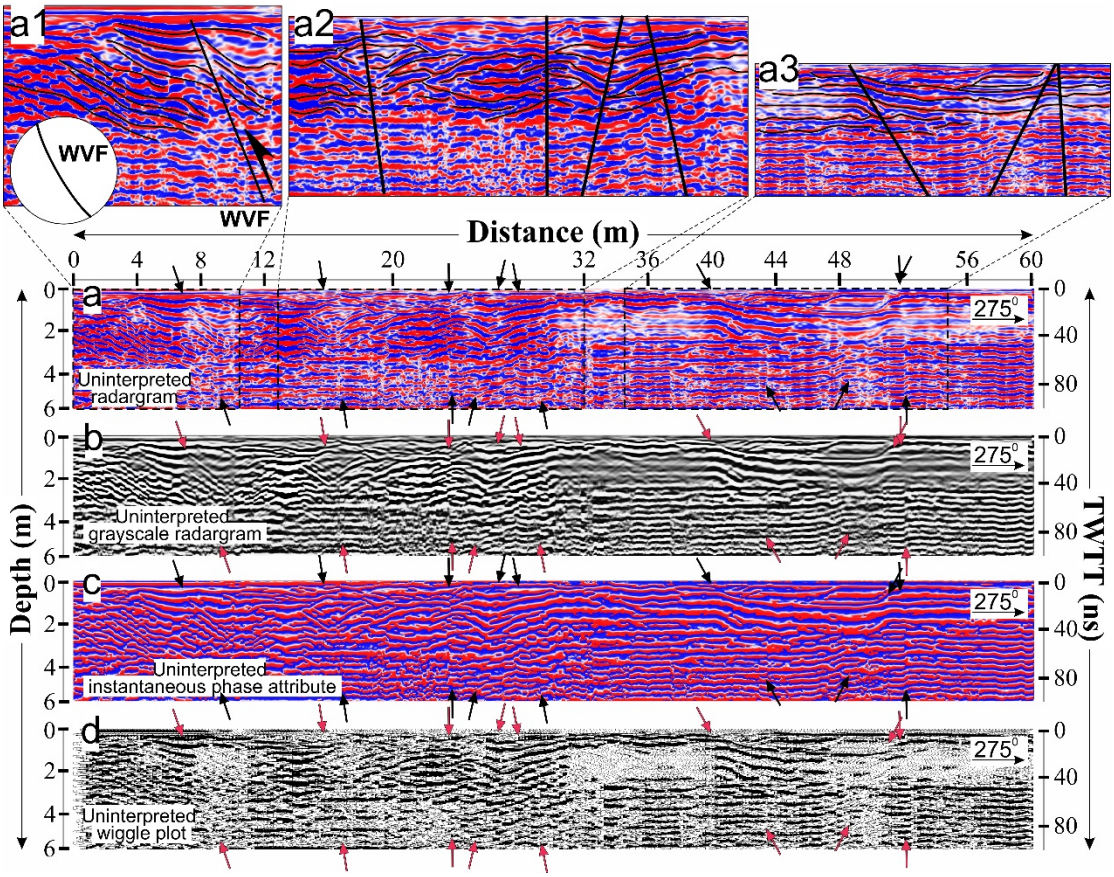

Fig. 6.2. (a) to (d) show uninterpreted radargram, uninterpreted grayscale radargram, uninterpreted radargram processed with instantaneous phase attribute and uninterpreted wiggle plot. Interpreted radar characteristics are shown in Figs (a1), (a2) and (a3). Axis on left side of the radargrams shows penetration depth in meters and on right side two-way travel-time (TWTT) in ns is denoted. The upper axis shows profile length (in meters) of the radargram. The presence of fault and deformation bands cluster are indicated by black arrows in Figs. (a) and (c), red arrows in Figs. (b) and (d).

The radargram is severely affected by sharp vertical bands of low-frequency from 40-100 ns depth. Also, the continuous, horizontal reflectors occurring below 40

ns depth are not clear and distinct. Therefore, processing of raw radargram is required as the data is affected by different kinds of noises during survey operation.

Full-pass background removal filter is applied to remove continuous, horizontal air wave and ground wave and also to remove bands of ringing noise below 50 ns depth occurring in the form of long, continuous horizontal bands. The background removal filter also corrected the reflector-geometry of alluvium (horizontal band) that continue up to ~1 m depth. The horizontal low-pass IIR filter of 7 scans is applied to remove sharp vertical low-frequency bands. The combination of vertical boxcar FIR low-pass filter of 410 MHz and high-pass filter of 150 MHz frequency is applied. It removed the left out low-frequency vertical bands and also, it made the reflectors below 40 ns depth more clear and visible. A 3 scan IIR horizontal low pass smoothing filter is applied to remove the snow-like noise and to further smooth the data. As the profiles are taken on flat terrain, there is no need to perform the topographic correction. The linear range gain is applied to improve the visibility of reflectors which has reduced during processing. Also, during acquisition, the shadow zone having very poor reflection response encountered from 10-50 ns depth occurring at intervals of 28-40 m and 48-60 m horizontal distance. To improve the visibility of these region, linear range gain is applied. Finally, the average velocity of 0.12 m ns^{-1} determined through CMP gather is used for time-depth conversion (Patidar et al., 2006). The attribute analysis using instantaneous phase based on Hilbert transform is performed on the processed radargram.

VIGODI FAULT (VF) AND ASSOCIATED SUBSIDIARY FAULTS

Site 12

At site 12, the VF can be identified at 7.5 m horizontal distance in the processed radargram. The fault is represented by truncation and offset of continuous reflectors (Figs. 6.1f-h). At the far side of field photograph in Fig. 6.1e, the SW dipping fault is exposed with ~0.5 m positive relief from the surrounding flat soil surface. The radargram can be divided into three distinct radar reflection packages:

(i) Thick, long, continuous reflector

At 0-25 ns depth interval, in the uppermost segment, the loose soil is represented by long, continuous, thick reflector (Fig. 6.1h).

(ii) Sub-horizontal reflectors package in footwall

At 0-7.5 m horizontal distance; long, continuous, horizontal to sub-horizontal reflectors belonging to Bhuj sandstone can be observed in the footwall. They are truncated along the SW dipping fault. The fault is marked by red continuous line in Fig. 6.1h.

(iii) Moderately dipping reflectors package in hangingwall

In the upthrown block, the radar reflections with ~20° dip towards SW, belonging to the deformed Bhuj sandstone are identified in the interval of 7.5-14 m horizontal distance. Reverse dip-slip is exemplified as the SW dipping reflectors in the hangingwall are displaced upward with respect to almost horizontal reflectors in the footwall (Fig. 6.1h). The multiple, green dashed lines represent the possible presence of deformation bands. They are identified by the offset and change in dip of continuous reflectors throughout the depth of profile. Due to the soil cover, their presence is not verified by the surficial exposure except the antithetic band 3. Almost horizontal, high amplitude, thick radar reflections throughout the depth of profile at 16-17 m horizontal distance are due to man-made utility buried underground (Fig. 6.1h).

The characteristic signatures of locating a fault plane are identified such as, truncation, thinning and dip change of radar reflector facies across the fault plane. Also, small hyperbolic diffraction at the tip of fault plane can be observed at 7.5 m horizontal distance. Thus, the near surface fault geometry and reverse slip-sense inferred from the GPR survey correlates well with the nearby surficial fault exposure.

GPR survey near site 13 – Vigodi Fault (VF)

In the central part, for ~4 km, the VF appears as ~30-50 cm high, NE dipping fault plane jutting out of the surrounding flat soil surface (Figs. 6.3a-c). In this segment, the VF is having patchy occurrence mostly buried below alluvial cover. To further authenticate our field observations, GPR survey was conducted near site 13, with 17 m profile length in N30° direction.

The radargram acquired across the VF was affected by sharp vertical bands of low-frequency. Also, it was showing long, continuous flat lying reflectors of ringing noise. The vertical position was adjusted by applying time-zero correction of 7 ns to remove the delay time and to match the surface position. The purpose of doing so was to get the accurate depth of reflectors because now the topmost scan of the radargram is in close approximation with the ground surface. The full pass background removal filter was applied to suppress the strong low-frequency noise. The vertical low-pass FIR

filter of 600 MHz cut-off frequency was applied which removed frequencies above the established threshold to a great extent. The horizontal low-pass smoothing IIR filter of 5 scans was then applied to reduce the snow-like noise and to remove the sharp vertical low-frequency bands.

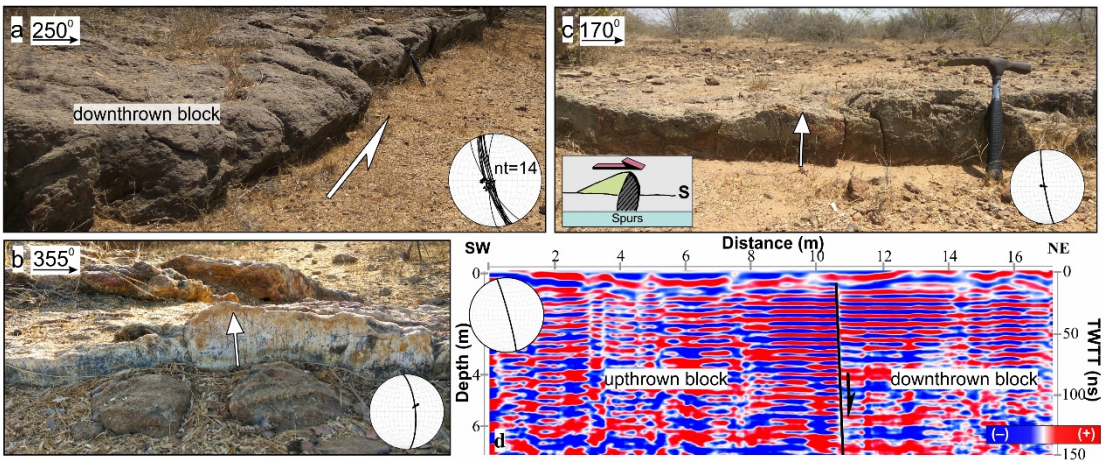

Fig. 6.3. (a)-(c) the SW dipping VF is exposed with ~0.5 m positive relief from the surrounding flat soil surface. Inset stereonet: 14 fault-slip data recorded. (d) 17 m long, NE directed GPR profile acquired using 200 MHz antenna across the NNW striking VF near site 13 (see Fig. 3.1 for location of GPR survey site). Interpreted radargram is shown with the axis on left side denote penetration depth in meters and on right side two way travel time (TWTT) in ns. The upper axis shows profile length in meters.

The processed radargram near site 13 shows almost horizontal reflections that are not because of the ringing noise but due to near-vertical dip nature of the fault plane. Almost vertical dipping fault is present at 10.5 m horizontal distance (Fig. 6.3d). The VF has been identified as sudden truncation of the horizontal reflectors across the fault plane (Fig. 6.3d). On the NE side of the VF (downthrown block), the truncated reflectors are displaced downwards with respect to the flat lying, horizontal reflectors in the upthrown block (Fig. 6.3d). The inferred fault geometry from the radargram doesn't match with the nearby surficial exposure of the VF at site 13 (Fig. 6.3). At the surface, the VF shows steep NE dipping fault plane while in the radargram, almost vertical fault plane is identified. However, the radargram helped in identifying the footwall lying on NE side and hangingwall on SW side indicating normal slip along the VF.

Site 14

At site 14, the SSW dipping, ~1.5 m high fault exposes the footwall block while the hanging wall block has moved up and eroded away. A shrine is built exactly over the NNW trending VF exposed in the Bhuj sandstone. Fault-slip analysis results suggest that the VF has generated under pure compressive stress regime with maximum horizontal principal stress (S_{Hmax}) trending in N20° E direction (Shaikh et al., 2020).

The 2D GPR survey is carried out ~120 m SSE of VF exposure, in order to understand the shallow subsurface nature of NNW trending VF and to further confirm our field observations indicating reverse dip-slip movement of the exposure of the VF (Fig. 6.4b). The shielded monostatic 200 MHz frequency antenna with single channel Subsurface Interface Radar-20 (SIR-20) system manufactured by GSSI Inc. USA is used to collect the radargrams in continuous mode (Fig. 6.4b). The survey wheel is connected to the antenna during survey operation. The dielectric constant is kept 7 with depth range of 100 ns and the depth of penetration achieved is 5 m. The marker is assigned manually to the radargram when the antenna crossed the approximate position of the fault-line. 46 m long profile is acquired in N240° direction perpendicular to the NNW trending VF.

The radargram recorded across the VF is severely affected by sharp vertical bands of low-frequency. Also, except the fault damage zone, the entire radargram shows continuous, horizontal reflectors with enormously high thickness which are masking the real reflections to a great extent. In the raw radargram, away from the fault zone, the two continuous, horizontal reflectors appears to be converging into single thick reflector at many places. Therefore, processing of raw radargram is required as the data is affected by different kinds of noises, instability of the equipment and vibrations during survey operations.

The post-survey processing is performed using RADAN (v.7) software by GSSI Inc. Time-zero correction is not applied to the radargram and reflectors dedicated to direct air wave and ground wave are retained in the processed radargram. The horizontal low-pass IIR filter of 7 scans is applied and it removed the sharp vertical low-frequency bands to a great extent. The combination of vertical FIR low-pass filter of 410 MHz and high-pass filter of 120 MHz frequency is applied which not only removed the left out low-frequency vertical bands but it also made the horizontal reflectors explicit and distinct. A 3 scan IIR horizontal low pass smoothing filter is applied to remove the snow-like noise and to further smooth the data.

As the profiles are taken on flat terrain, there is no need to perform the topographic correction. The linear range gain is applied to artificially increase the amplitudes of radar signals, to offset the attenuation caused during processing described earlier. Finally, the average velocity of 0.12 m ns^{-1} determined through CMP gather is used for time-depth conversion (Patidar et al., 2006).

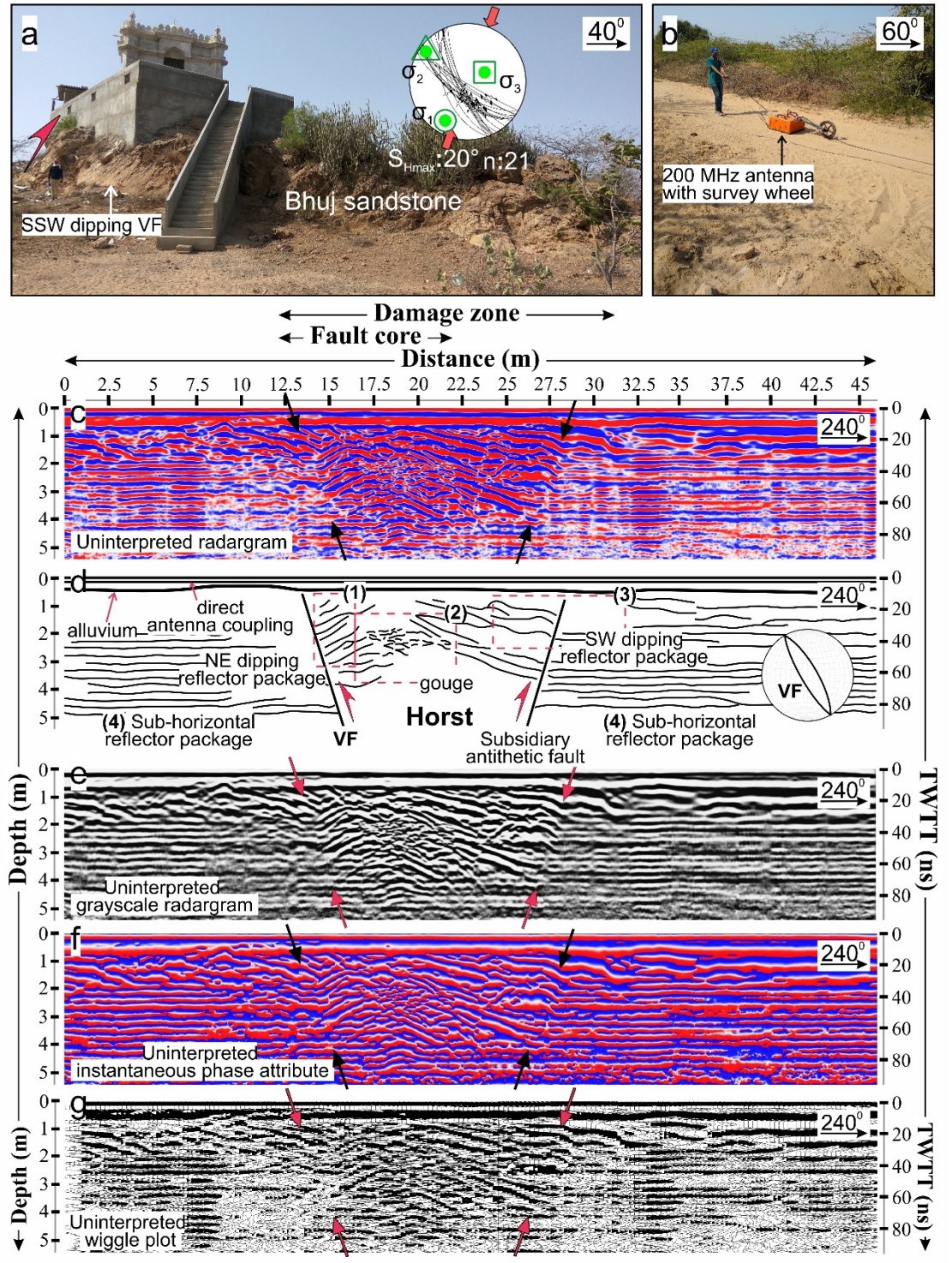

Fig. 6.4. (a) Exposure of NW trending VF with reverse slip in Bhuj sandstone at site 14 formed under pure compressive stress regime. The red half-arrow indicates the upward motion of the missing block (hangingwall). Height of the person is 188 cm as scale. Inset paleostress tensor (lower hemisphere, equal-area projection) deduced by Right Dihedral Method (RDM) implemented in Win_Tensor (Delvaux and Sperner, 2003) software is shown. Black lines: fault planes with slip vectors (marked by open circles with arrows) (n = 21). Red arrows pointing inward: the orientation of maximum horizontal principal stress (S_{Hmax}). Green circle, triangle and square: orientation of maximum (σ_1), intermediate (σ_2) and minimum (σ_3) stress axes respectively ($\sigma_1 \geq \sigma_2 \geq \sigma_3$). (b) ~120 m SSE of site 14, person dragging the 200 MHz antenna with survey wheel attached to it in SW direction, perpendicular to approximate trend of the VF. (c)-(g) show uninterpreted radargram, interpreted radar facies, uninterpreted grayscale radargram, uninterpreted radargram processed with instantaneous phase attribute and uninterpreted wiggle plot. Axis on left side of the radargrams shows penetration depth in meters and on right side two-way travel-time (TWTT) in ns is denoted. The upper axis shows profile length (in meters) of the radargram. At ~13 m horizontal distance, the VF can be identified due to sudden change in dip of the continuous reflectors. Both the faults are indicated by black arrows in Figs. (c) and (f), red arrows in Fig. (e) and white arrows in Fig. (g). The radargram processed with instantaneous phase attribute marks the clear offset and change in dip of the continuous reflectors along the VF as well as along the antithetic fault.

The attribute analysis using instantaneous phase based on Hilbert transform is performed on the processed radargram. The NNW trending and SSW dipping VF can be identified at 13 m horizontal distance in the processed radargram.

Across the fault plane, there is a sudden change in the dip of reflectors in the hangingwall block. Whereas, in the footwall block, almost horizontal reflector patterns are observed. No thinning/thickening of reflectors is observed across the fault plane. The radargram can be divided into four distinct radar reflection packages demarcated on the basis of its reflector pattern response:

(1) NE dipping reflector package: At ~15 m horizontal distance, the high amplitude, NE dipping parallel to sub-parallel set of radar reflections (dip amount: 30-50°), prominent in the hangingwall of the SW dipping VF, highlighted by red dashed box area (1) (Fig. 6.4d). The NE dipping reflectors in the hangingwall of the VF are riding over (displaced up) the SW dipping/sub-horizontal reflectors in the footwall indicating reverse slip along the VF.

(2) Chaotic radar reflection package: In the middle segment of the radargram, a package of thin, small, discontinuous reflectors with no specific shape and

highly variable dip can be observed in the hangingwall block of the VF between 2-4 m depth (40-60 ns depth range) (Fig. 6.4d). This chaotic radar reflection package indicate the presence of deformed and fragmented but intact lenses of host Bhuj sandstone derived from the principal slip surface and this zone can be collectively called as sandstone gouge consisting of non-cohesive crushed material, highlighted in the dashed box area (2).

(3) SW dipping reflector package: The SW dipping reflector package (dip amount: 5-30°), highlighted in the dashed box area (3) shows the thick, long reflectors with high amplitude signals. They show sudden change in dip/warping and thinning of reflectors at ~28 m horizontal distance which marks the presence of subsidiary, antithetic fault with reverse slip (Fig. 6.4d). The gently SW dipping reflectors in the hangingwall of the antithetic fault becomes sub-horizontal to horizontal in the footwall. The two oppositely dipping reverse faults marks the presence of the uplifted horst from ~13-28 m horizontal distance.

It can be observed that the amplitude of reflectors suddenly increases at ~14 m horizontal distance that continuous up to 32 m. This zone of high amplitude radar reflections, which is identified as horst region, also demarcates the limit of fault damage zone which cannot be ascertained by field observations. The reflector pattern facies (1), (2) and (3) together constitute the fault damage zone. The approximate width of the fault damage zone is ~18 m.

The reflector package (1) and (2) represents the high-strain zone where most of the displacement and deformation is accommodated. Therefore, these two assemblages demarcate the fault core of the SSW dipping VF.

(4) Horizontal/sub-horizontal reflector package: Beyond the fault damage zone width (<12.5 m and >28 m horizontal distance), essentially horizontal reflection pattern with comparatively low amplitude reflection facies are observed which belong to undeformed, horizontal beds of Bhuj sandstone.

GUGRIANA FAULT (GUF) AND ASSOCIATED SUBSIDIARY SYNTHETIC FAULT

Site 15

At site 15, THE GUF is exposed east of NNW trending asymmetrical hill range (with steep eastward and gentler westward slope) (Fig. 6.5). Locally, the GUF appears to be of having curved geometry with strike ranging between N140°-N190° E. The

WSW dipping striated GUF is showing reverse slip as the missing block (footwall) has moved down with respect to the exposed hanging wall (Figs. 6.5a, b, c).

Sub-horizontal reflector package (1) encompasses long, continuous horizontal to sub-horizontal reflection pattern with moderate to high amplitude reflection facies.

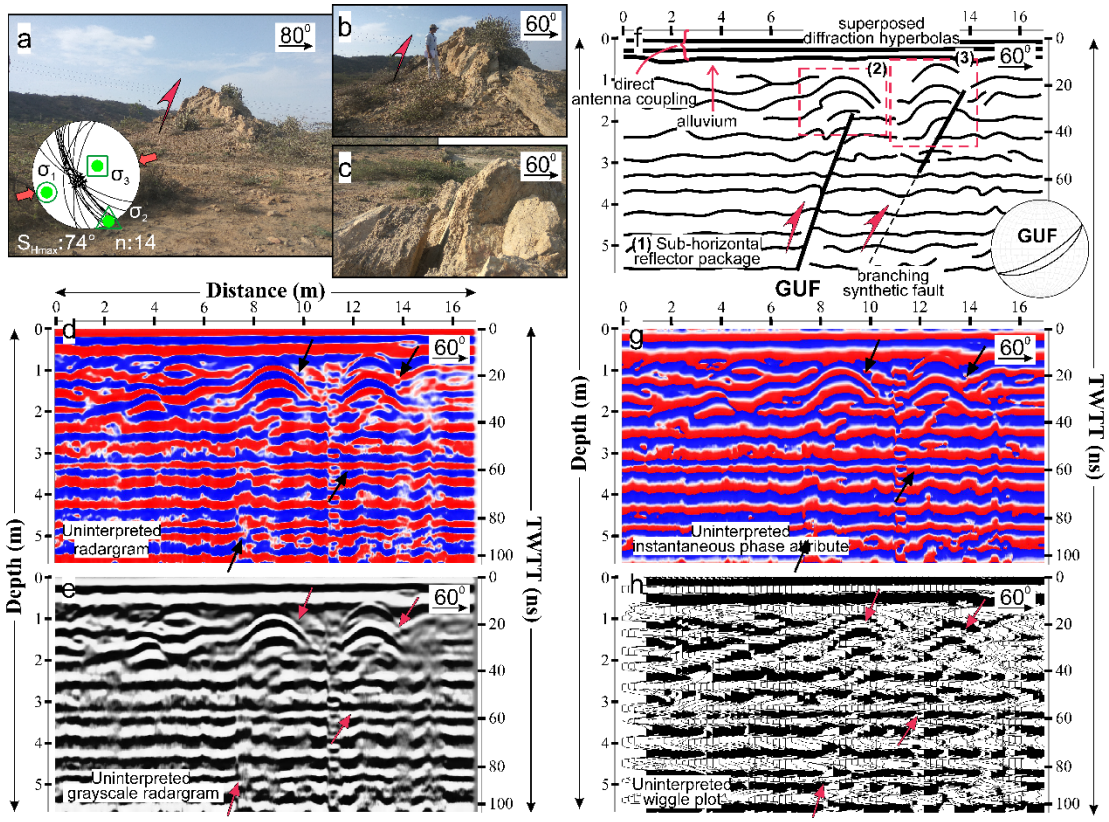

Fig. 6.5. (a) to (c) Regional-view of NNW trending GUF with reverse slip exposed in Bhuj sandstone. The red half-arrow indicates the upward motion of the missing block (hangingwall). Inset paleostress tensor (lower hemisphere, equal-area projection) deduced by Right Dihedral Method (RDM) implemented in Win-Tensor (Delvaux and Sperner, 2003) software is shown. Black lines: fault planes with slip vectors (marked by open circles with arrows) (n = 14). Red arrows pointing inward: the orientation of maximum horizontal principal stress (S_{Hmax}). Green circle, triangle and square: orientation of maximum (σ_1), intermediate (σ_2) and minimum (σ_3) stress axes respectively ($\sigma_1 \geq \sigma_2 \geq \sigma_3$). (d)-(h) show uninterpreted radargram, uninterpreted grayscale radargram, interpreted radar facies, uninterpreted radargram processed with instantaneous phase attribute and uninterpreted wiggle plot. Axis on left side of the radargrams shows penetration depth in meters and on right side two-way travel-time (TWTT) in ns is denoted. The upper axis shows profile length (in meters) of the radargram. The GUF can be located at ~10 m horizontal distance due to displacement along continuous, horizontal reflectors. Another subsidiary synthetic fault with reverse slip can also be located towards the footwall side of the GUF. Both the faults are indicated by black arrows in Figs. (d) and (g), red arrows in Figs. (e) and (h).

They are observed in the GPR profile below ~3 m depth of the radargram. The reflectors package (2) and (3) exhibit a series of convex reflections with moderate to high amplitude responses. They are exclusively located in the upper parts of the radargram. On the top, they are covered by thin alluvial cover, which is masking their surficial exposure.

In the processed radargram, two diffraction hyperbolas can be observed. They represent a duplex structure with two horses can be clearly observed. Usually, diffraction hyperbolas form at the tip of the fault plane and in such cases, diffraction hyperbolas should not be considered as true reflections. They should be collapsed using migration filter during post-processing of GPR data. But, superposed hyperbolas are found at the tip of both the fault planes and they represent the folded surface and therefore, they should be considered as true reflections. The structure thus formed represents a fault propagation fold. The radargram processed with instantaneous phase attribute marks the clear offset and change in dip of the continuous reflectors along the GUF as well as along the synthetic fault. The upward propagating GUF and subsidiary synthetic fault lost their slip and terminated in the shallow subsurface by passing their shortening to a fold forming at their tips.